7-2014

Tuned to Resonance

Dimitrios Peroulis
Purdue University, Birck Nanotechnology Center, dperouli@purdue.edu

Eric Naglich
US Naval Research Laboratory

Michael Sinani
Purdue University, Birck Nanotechnology Center, msinani@purdue.edu

Mark Hickle
Purdue University, Birck Nanotechnology Center, mhickle@purdue.edu

FOCUSED ISSUE FEATURE

Tuned to Resonance

Dimitrios Peroulis, Eric Naglich, Michael Sinani, and Mark Hickle

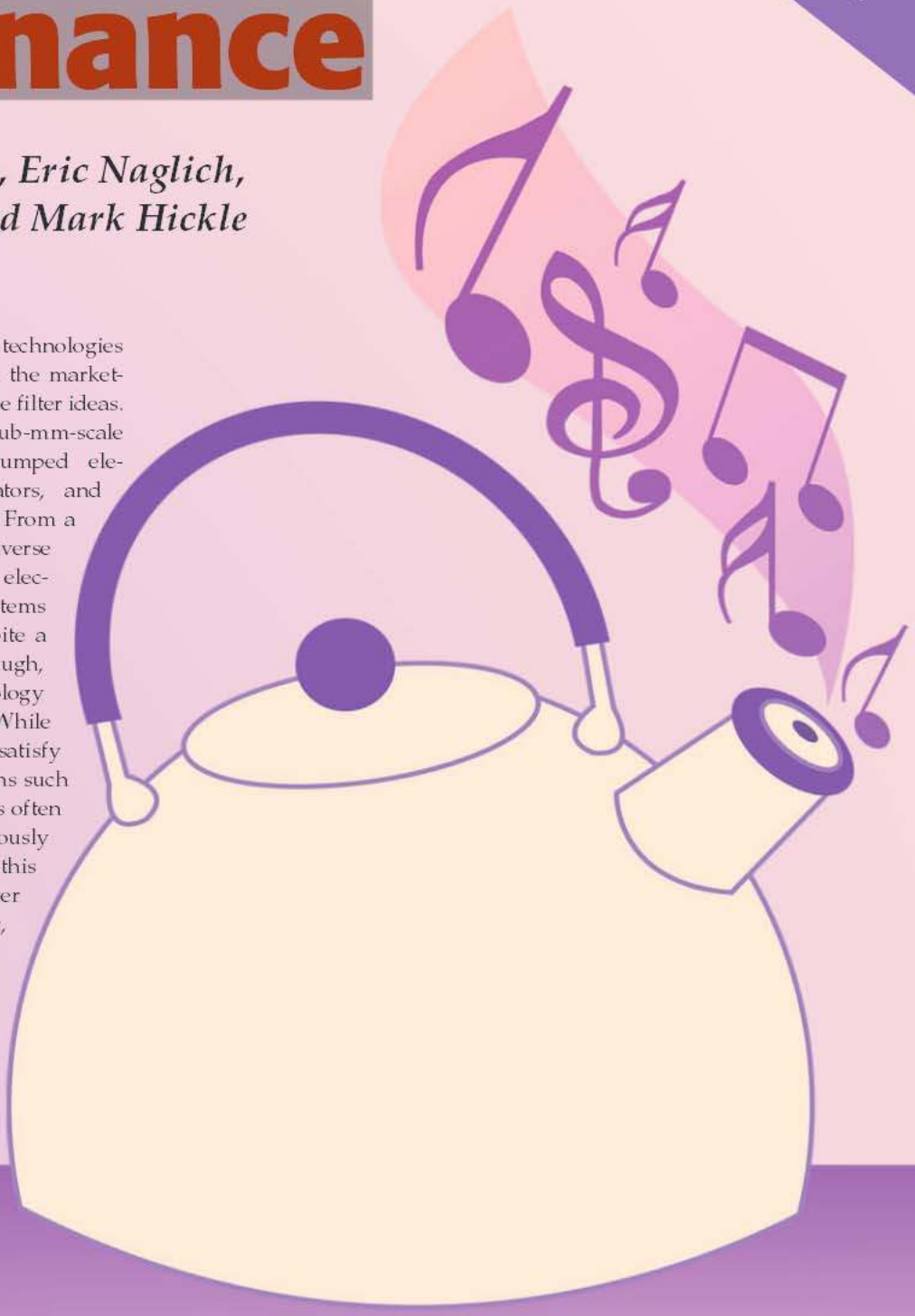

A number of promising technologies can be found today in the marketplace of reconfigurable filter ideas. They range from sub-mm-scale acoustic filters, lumped elements, two-dimensional resonators, and full three-dimensional solutions. From a system perspective, an equally diverse pool of communication, radar, electronic warfare, and sensing systems need reconfigurable filters. Despite a strong demand for such filters though, it is not easy to identify a technology that satisfies all requirements. While it is relatively straightforward to satisfy one or two important specifications such as low loss or high selectivity, it is often quite challenging to simultaneously satisfy all of them. For instance, this is particularly true when low power consumption, small form factor, and low loss become simultaneously critical decision factors. Several combinations of such factors can result in necessary design tradeoffs with no obvious solutions. Table 1 summarizes

Dimitrios Peroulis (dperouli@purdue.edu), Michael Sinani, and Mark Hickle are with the School of Electrical and Computer Engineering, Birck Nanotechnology Center, Purdue University, West Lafayette, Indiana, United States. Eric Naglich is with Code 6851 U.S. Naval Research Laboratory, Washington, D.C., United States.

Digital Object Identifier 10.1109/MMM.2014.2321103
Date of publication: 11 July 2014

TABLE 1. Reconfigurable filter technology: Common deciding factors.

Insertion loss and return loss
Isolation and ultimate rejection
Bandwidth and selectivity
Transmission zeros: existence and tunability
Form factor (volume, footprint, weight)
RF power handling
Power consumption
Linearity
Tuning speed
Control mechanism and implementation circuitry
Fabrication, assembly, and tuning cost
Integration with other technologies (e.g., CMOS)
Filter input impedance versus tuning
Analog versus digital tuning
Vibration, shock, temperature sensitivity
Reliability (cycling, constant loading)
Tuning voltage noise immunity

several common deciding factors in selecting a reconfigurable filter technology.

The situation becomes even more demanding when we don't restrict our focus on frequency-tunable filters, which are the most common class of reconfigurable filters, but we rather consider transfer-function-adaptive filters that have the capability to reconfigure their entire transfer function. For example, when a radio-frequency (RF) tunable filter is reconfigured to reject multiple frequency- and amplitude-unknown interferers, tuning its center frequency may be insufficient. As a result, it may be necessary to reconfigure its entire transfer-function in the field.

It is important to recognize that existing technology capabilities allow for such filters to be designed and implemented with cost-effective fabrication techniques. The evanescent-mode cavity filter technology is one of the best examples to demonstrate this. This is because it provides a natural optimization of most of the critical features summarized in Table 1. For example, it provides a wide tuning range (>2:1) with a graceful quality factor degradation in a relatively small form factor.

Fundamental Technology Characteristics

The evanescent-mode cavity resonator is the first critical building block of the presented technology. Such a resonator can be constructed by inserting a metallic

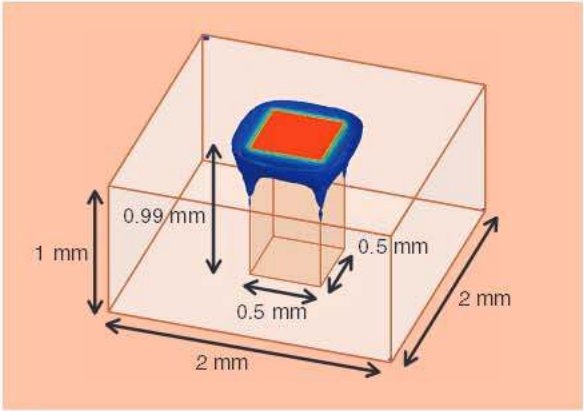

Figure 1. *Electric field distribution in the loaded cavity resonator (f_0 = 18.6-GHz).*

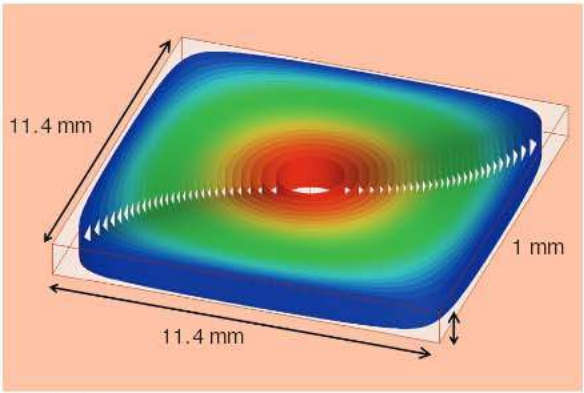

Figure 2. *Electric field distribution in the unloaded cavity resonator (f_0 = 18.6-GHz).*

obstacle (post) in the middle of the cavity (Figure 1). This cavity-loading technique has been well known and has resulted in a whole generation of hand-tuned filters in the 1970s until today [1]–[17]. In fact, researchers also refer to this technology as coaxial or combline resonators. However, heavily loading the resonator with a post that nearly touches the top cavity wall results in three main effects:

- *Miniaturization*: For example, a loaded $2\times2\times1\,\text{mm}^3$ cavity with a $0.5\times0.5\times0.99\,\text{mm}^3$ center post resonates at 18.6-GHz (Q = 700), while the same cavity resonates at 106-GHz without the post. This represents a 97% volume reduction in the sense that a 18.5-GHz unloaded cavity would be $11.4\times11.4\times1\,\text{mm}^3$ (Q = 1,800). These are depicted in Figures 1 and 2.
- *Tuning*: The existence of the post allows for the electric field to be concentrated in an area that is amenable to practical tuning means. For example, approximately 91% of the electric field energy is concentrated over the post area in the aforementioned loaded $2\times2\times1\,\text{mm}^3$ cavity with a $0.5\times0.5\times0.99\,\text{mm}^3$ center post. A tuning element such as a bendable diaphragm can be inserted at this point of concentrated electric field,

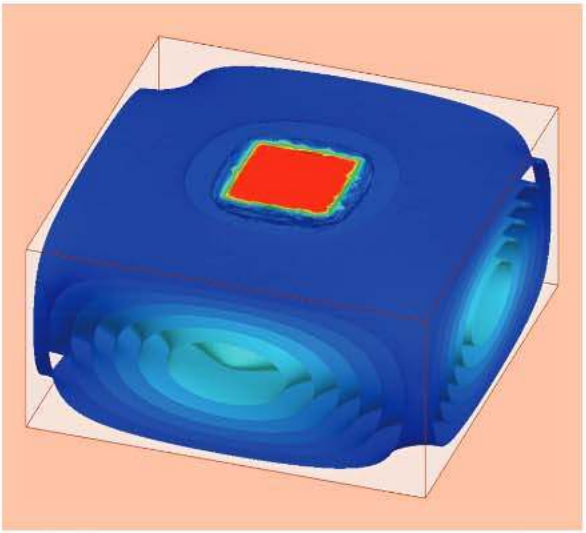

Figure 3. *First spurious mode of loaded cavity* (f_1 = 152-GHz).

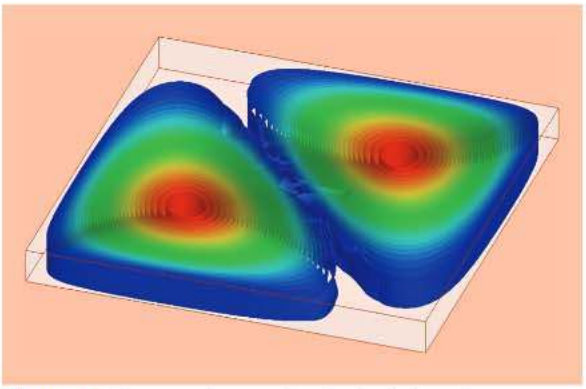

Figure 4. *First spurious mode of unloaded cavity* (f_1 = 29.4-GHz).

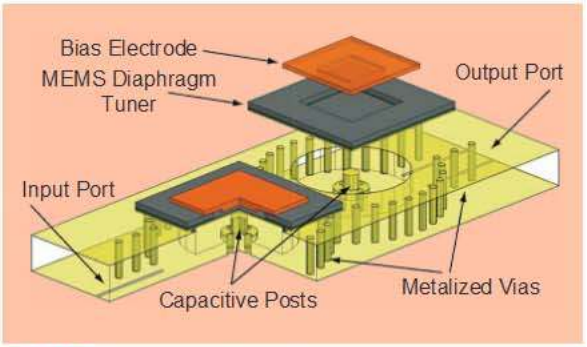

Figure 5. *A tunable substrate-integrated waveguide-based evanescent-mode filter. The cavities and posts are defined by metalized vias, and a custom MEMS electrostatic actuator is implemented to enable wide tuning range. (Drawing originally from [4]).*

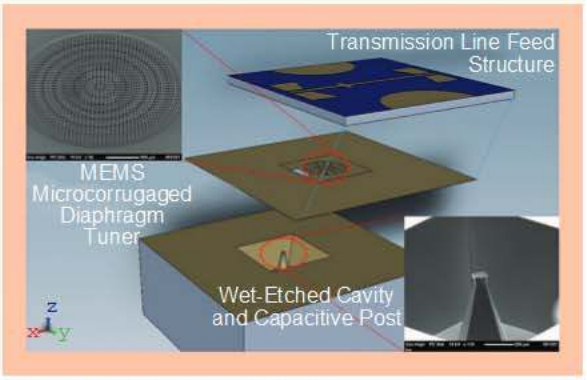

Figure 6. *W-Band tunable bandstop-configured resonator featuring a low-voltage MEMS electrostatically actuated tuning element, a capacitive post, and cavity fabricated using high-precision silicon wet-etching techniques. (Drawing originally from [25].)*

and can greatly influence the resonant frequency with a small displacement. Resonators have been demonstrated which exhibit a 4:1 tuning range by displacing a microelectromechanical systems (MEMS) diaphragm by 15 nm [2].

- *Wide spurious free range*: It is possible to design loaded resonators with a greater than 35:1 spurious free range [3] while the spurious free range of a typical unloaded cavity resonator is less than 2:1 (Figures 3 and 4).

Fabrication Technologies: From Sub-GHz to W-Band

Tunable evanescent-mode cavity resonators consist of cavities loaded with tunable capacitive objects, and as such they can take many forms and can be realized with different fabrication techniques. The various fabrication techniques offer tradeoffs in term of complexity, performance, reliability, and cost. The most common fabrication method of evanescent cavity-based filters is based on the principles of substrate-integrated waveguides. Cavities loaded with capacitive posts are established by creating a boundary of metalized via holes, and electromechanical actuators such as piezoelectric transducers or flexible RF MEMS diaphragms are attached to the top of the cavity with a small gap of a few μm between the capacitive post and the actuator (Figures 5 and 6). Changing this gap modifies the loading capacitance of the resonator, and with careful choice of initial gap the frequency of the resonator can be very widely tuned (3.5:1 is reported in [5]) with only tens of microns of actuator displacement. This robust and proven fabrication method offers good performance and has been used to create multiplexers [6], bandpass and bandstop filters [4], [10]–[16], filter cascades [14], and high-efficiency tunable RF power amplifiers [17]. It has the advantage of relative simplicity, as it can be fabricated using readily available machining tools. However, the limited precision of such tooling has limited filters based on this technology to <6–10-GHz.

In an effort to overcome the limitations of the substrate-integrated waveguide fabrication technology, a push has recently been made toward fabricating tunable evanescent-mode filters with silicon

Achieving a widely tunable, low-power, and high-Q resonator with wide spurious free range in a mobile form factor is possible with the evanescent-mode cavity technology.

micromachining techniques. The well-characterized silicon micromachining methods which have been employed for many years in the fabrication of MEMS can yield very precise devices, in some cases with submicron critical dimensions. This degree of precision has enabled record-performance resonators, with reported results such as a 6–24-GHz resonator with a quality factor of 300–1000 [2], [24], and a 70–80-GHz resonator with a quality factor of over 400 [25]. The batch fabrication aspect of silicon micromachining lends filters based on such technology the potential to be mass-produced at low cost. These filters have the additional advantages of a) silicon-to-silicon integration, and b) contact-free operation that makes them immune to contact-based failures commonly found in RF MEMS switches. Additional research is needed to find optimal tradeoffs between fabrication parameters, mechanical/thermal performance, and RF characteristics.

An additional class of evanescent-mode filter technology combines conventionally machined cavities with RF-MEMS tuning elements such as cantilever-beams (Figure 7) [18], RF-MEMS varactors [19], or switched capacitor networks [20]. This technology utilizes relatively straightforward and well-characterized MEMS fabrication of cantilever actuators and capacitors, and has yielded devices with moderately high-quality factors and tuning ranges.

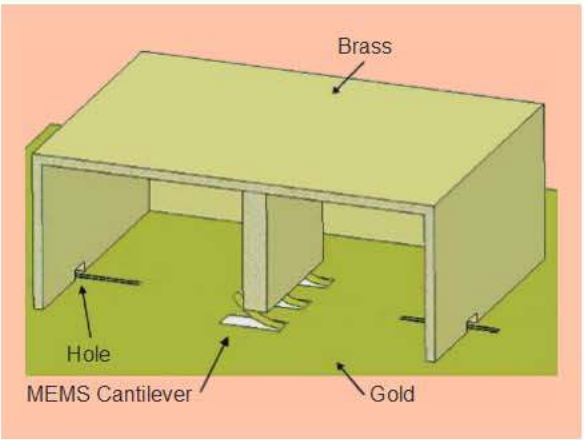

Figure 7. *A conventionally machined evanescent-mode cavity loaded with three MEMS cantilever tuning elements. (Drawing after [18].)*

From the Coupling Matrix to Practical Implementations

Of the multiple theoretical methods used to design filters, the coupling matrix is one of the most powerful for the design of practical reconfigurable filters [26]. The coupling matrix method models all resonators of a filter to be identical (although they may resonate at different frequencies), which is advantageous in fabrication, while completely specifying a filter's transfer function through the adjustment of coupling values between identical resonators. The method also provides simultaneous solution of all of the theoretical filter design parameters, removing the need for element-by-element solving associated with some filter design techniques. Finally, the coupling matrix provides an intuitive way to show which parameters must be changed in order to reconfigure a filter's transfer function from one type to another. It will therefore be used to both design and describe reconfigurable filters in this article.

The coupling matrix method involves formulating the frequency- and port-impedance-normalized model of a filter network shown in (1).

$$Z = R + jM + U. \tag{1}$$

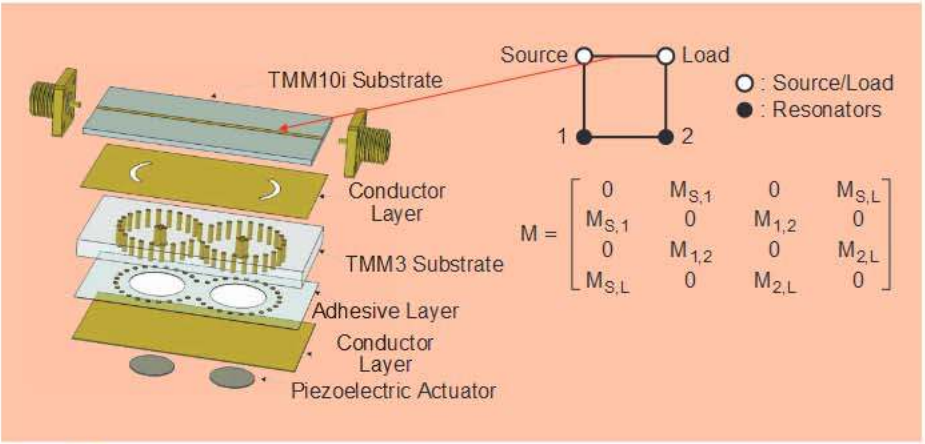

Figure 8. *A separated view of a substrate integrated evanescent-mode cavity two-pole bandstop filter, its coupling-routing diagram, and its coupling matrix.*

In (1), `Z` is the impedance matrix of the network, `R` models the resistive terminations of external ports to the network, `j` is the square root of −1, and `U` models the frequency behavior of the resonators. `M` models the coupling between network elements and is named the coupling matrix. Matrices for the example two-pole bandstop filter shown in Figure 8 are shown in (2).

$$R = \begin{bmatrix} 1 & 0 & 0 & 0 \\ 0 & 0 & 0 & 0 \\ 0 & 0 & 0 & 0 \\ 0 & 0 & 0 & 1 \end{bmatrix}$$

$$M = \begin{bmatrix} 0 & M_{s,1} & 0 & M_{s,L} \\ M_{s,1} & 0 & M_{1,2} & 0 \\ 0 & M_{1,2} & 0 & M_{2,L} \\ M_{s,L} & 0 & M_{2,L} & 0 \end{bmatrix}$$

$$U = \begin{bmatrix} 0 & 0 & 0 & 0 \\ 0 & s & 0 & 0 \\ 0 & 0 & s & 0 \\ 0 & 0 & 0 & 0 \end{bmatrix} \tag{2}$$

Note that the 1 s in the R matrix correspond to ports with normalized 1 Ω impedance and that the s's in the U matrix represent $j\omega$, where ω is radian frequency. $M_{a,b}$ values represent coupling from network element a to network element b, where network elements can be ports, resonators, etc. The relative strengths and signs of the $M_{a,b}$ values specify the filter transfer function in this formulation. The transfer function of the network can be solved for from (1) and matched to the desired filter polynomial response.

Figure 8 shows a separated view of a two-pole bandstop filter that uses evanescent-mode cavity resonators, its coupling-routing diagram, and its coupling matrix. In order to physically realize such a filter from a coupling matrix, each coupling value, $M_{a,b}$, must be extracted from simulations. External coupling values, which are represented as $M_{s,1}$ and $M_{2,L}$ in the matrix in Figure 8, can be extracted from the phase response of a simulation of a resonator with a single port. After de-embeding the port face so that the 0° phase crossing is at the resonant frequency, $M_{s,1}$ can be determined from

$$f_2 - f_1 = M_{s,1}^2 D, \tag{3}$$

where $f_2 - f_1$ is the difference in frequency between the positive and negative 90° phase points around resonance in the S_{11} response and D is the design fractional bandwidth. Interresonator coupling values, which are represented as $M_{1,2}$ in the matrix in Figure 8, can be extracted from the magnitude response of a simulation of two resonators each with a weakly coupled port. $M_{1,2}$ can be determined from

$$f_2 - f_1 = M_{1,2} D, \tag{4}$$

where $f_2 - f_1$ is the difference in frequency between the peaks in the weakly coupled S_{21} response and D is the design fractional bandwidth. Using simulation and (1)–(4), one can design and describe many types of reconfigurable filters.

Center-Frequency-Tunable Filters

Filters with tunable center frequencies are probably the simplest class of reconfigurable filters and can be implemented by integrating frequency-tunable resonators with traditional filter synthesis methods. When designing filters whose only reconfigurability is center-frequency tuning, the most important design objectives are typically low insertion loss, high selectivity, and retaining a desired filter shape over a wide tuning range. Meeting such requirements necessitates the use of resonators which maintain high-quality factor over a wide tuning range—characteristics which are uniquely provided by evanescent-mode cavity resonators. Tunable evanescent-mode resonators are typically capable of achieving quality factors between 500 and 1,000 and tuning ranges greater than 2:1 (Figure 9). This represents an order of magnitude improvement over tunable microstrip resonators, whose quality factors are often around 50–100 for similar tuning ranges. These high-performance characteristics make evanescent-mode resonators well suited for applications in low

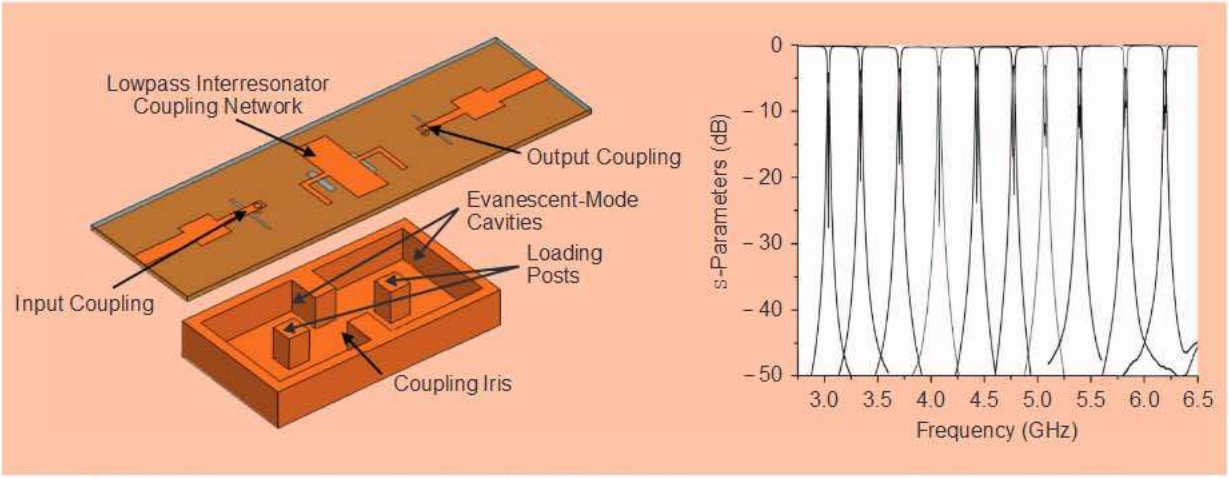

Figure 9. *A 3-6-GHz evanescent-mode bandpass filter. This filter features a very narrow and nearly constant 0.5% fractional bandwidth, while maintaining less than 4-dB of insertion loss across its tuning range [29].*

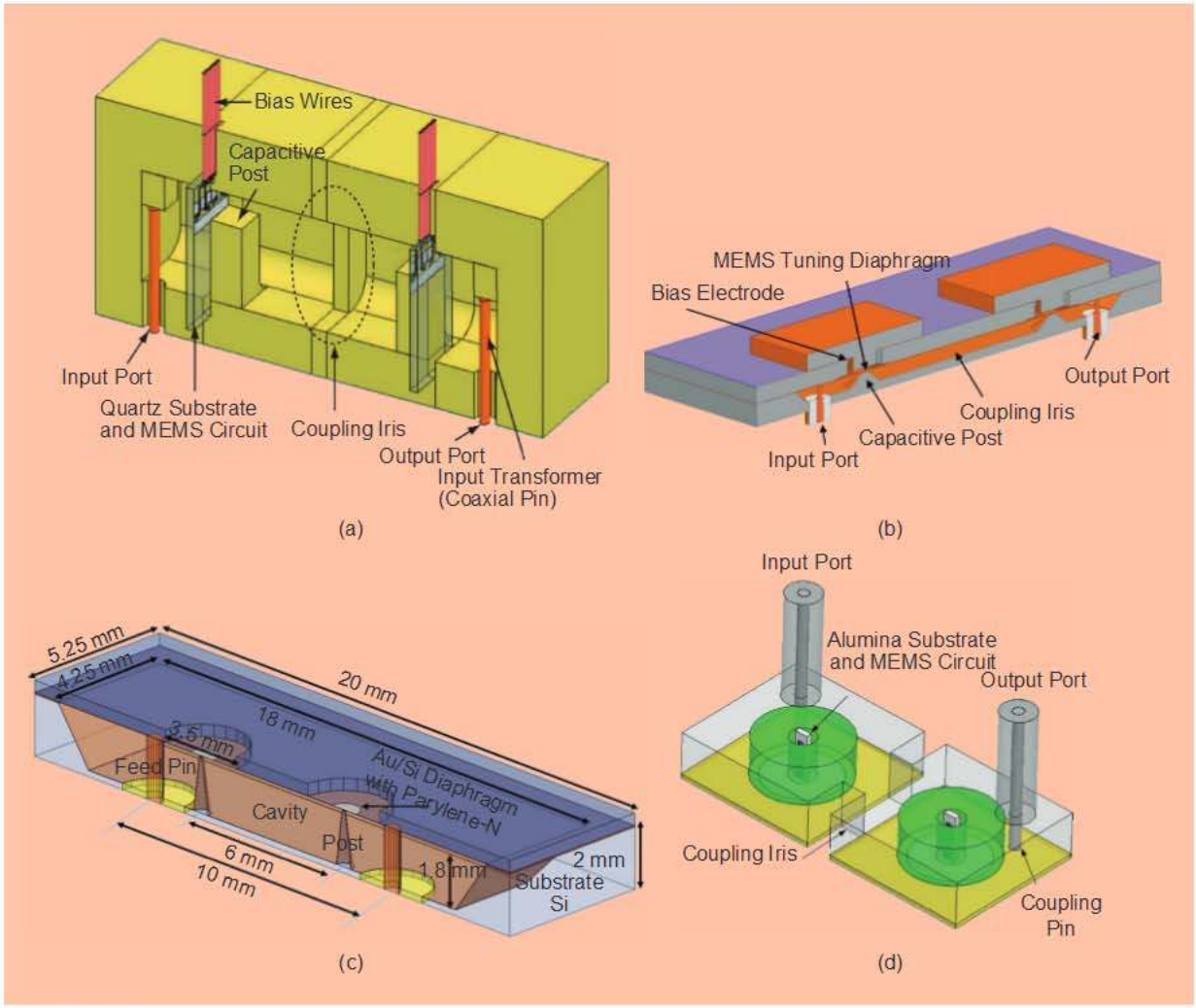

Figure 10. *Tunable bandpass filter examples. (a) 2.4–2.6-GHz tuning range, 1% fractional bandwidth with 4.9–3.2-dB insertion loss. Extracted Q = 350–500 [19]. (b) 23–35-GHz tuning range, 0.9–4.0% bandwidth with 4.2–1.5-dB insertion loss. Extracted Q = 550–750 [27]. (c) 6.7–20.5-GHz tuning range, 10–17% bandwidth with less than 0.66-dB insertion loss across tuning range. Extracted Q = 380–1010 [28]. (d) 5.0–5.2-GHz tuning range, 0.5% bandwidth with less than 2.8-dB insertion loss. Extracted Q = 550–800 [22]; see also [44] for this technology.*

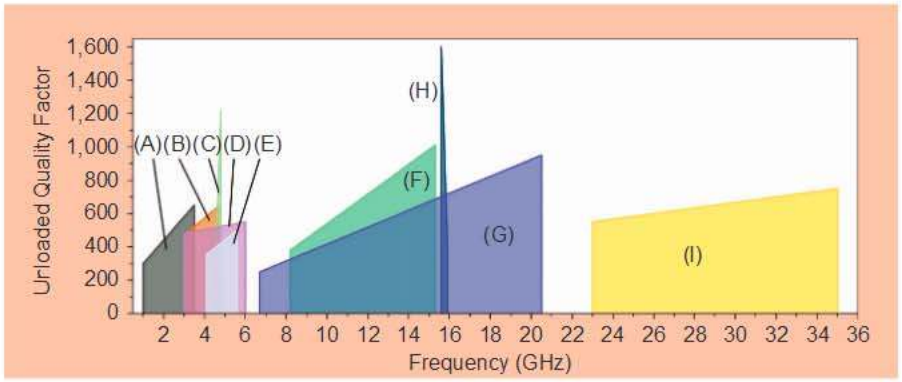

Figure 11. *A summary of state-of-the-art two-pole tunable filter performance. (A) Moon et. al [5], (B) Liu et al. [4], (C) Huang et al. [22], (D) Joshi [29], (E) Park et al. [19], (F) and (G) Arif et al. [28], (H) Yan et al. [21]; see also [45] for this technology, (I) Yang et al. [27].*

loss, widely tunable filters. Figures 10 and 11 present a summary of the performance obtained by state-of-the-art tunable filters.

One primary drawback of the current generation of center frequency tunable filters is the difficulty in maintaining constant filter shape across their tuning range. The frequency-dependent variation of external and interresonator couplings causes the bandwidth to change and the transfer function to degrade as the filter's center frequency is tuned. This becomes increasingly problematic as the tuning range is increased, with some examples showing more than a 300% increase in fractional bandwidth over a 1.5:1 tuning range [27]. This problem has been addressed

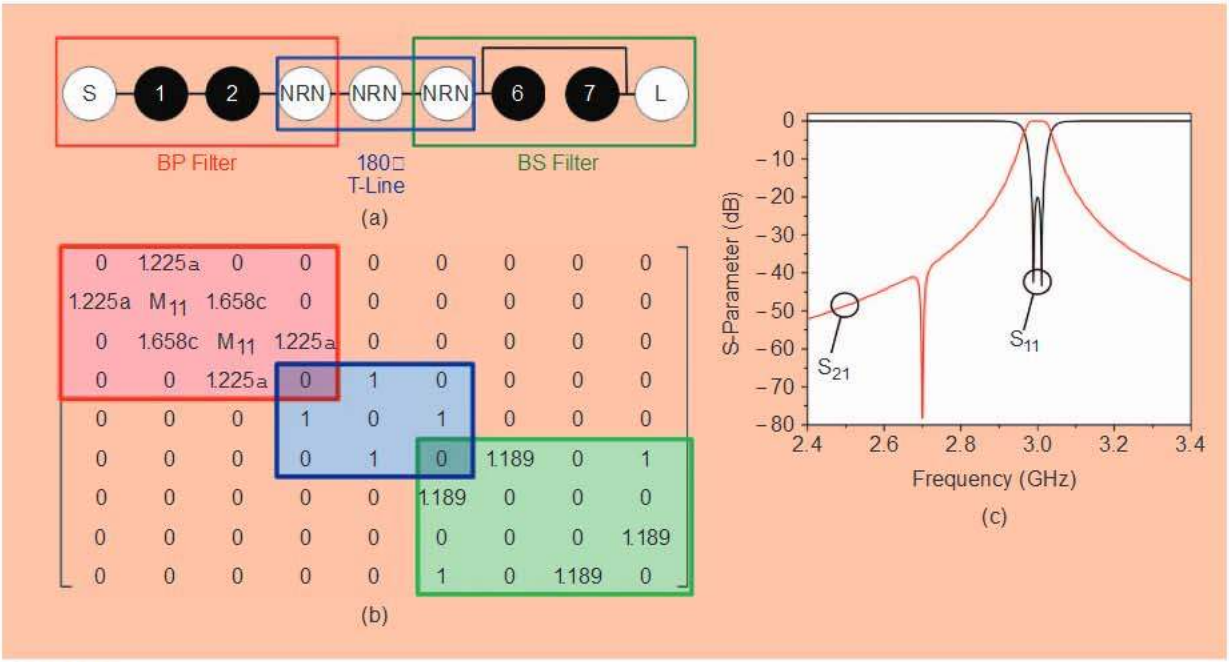

Figure 12. *(a) Coupling-routing diagram with subcircuit color-coded boxes of a two-pole bandpass filter cascaded with a two-pole bandstop filter using a 180° transmission line. (b) Coupling matrix for (a). (c) Synthesized frequency-scaled and shifted response. NRN = Nonresonating Node.*

by the use of tunable couplings [29], but this increases design and fabrication complexity and requires additional control voltages. It is often desirable to use coupling structures which have little or no variation with frequency.

Filter Cascades for Interference Mitigation

While the filters presented in the previous section have wide tuning ranges, high-quality factors, and innovative fabrication technologies, there may be applications where higher and more targeted isolation are required. Additionally, as cognitive and spectrally aware radio architectures are advanced, they may become capable of determining the location of interfering signals in the spectrum that have the highest chance of adversely affecting a receiver. While the filters in the previous section would allow a receiver to shift its operating frequency to a band that was away from the strongest interference, such a strategy might not provide sufficient isolation or may require unattractive performance tradeoffs in order to obtain the required amounts of isolation. For example, when strong interferers appear near the passband, a filter may have to contain a large number of poles in order to provide enough attenuation of the strong interference. While such a design is often used, it also adds significant insertion loss to the filter response.

In scenarios with few strong interferers, cascades of bandpass and bandstop center-frequency-tunable filters offer the significant advantage of lower insertion loss while still providing large amounts of targeted isolation. For example, a two-pole bandpass filter could be cascaded with a two-pole bandstop filter using a 180° transmission line. This configuration is shown in Figure 12(a).

The coupling matrix for this circuit is shown in Figure 12(b). Note that a and c are scaling factors that allow the bandpass and bandstop filters to have different design bandwidths [14]. A synthesized frequency-scaled and shifted response is shown in Figure 12(c), where the bandpass filter and the bandstop filter have different bandwidths. The two-pole bandpass filter response at 3-GHz has a low-loss passband and provides some isolation from frequencies away from the passband. However, if this amount of isolation is not adequate for a large signal, a bandstop response can be tuned to the frequency of the large signal, significantly increasing the local attenuation. In Figure 12(c), the attenuation is increased from approximately 40-dB to very deep attenuation over a narrow bandwidth.

The passbands and notch stopbands in configurations such as the one in Figure 12 can be tuned over wide frequency ranges while still producing responses similar to the one in Figure 12(c). Although issues can arise from resonances of the connecting transmission line or impedance mismatch between the output impedance of the bandpass filter and the input impedance of the bandstop filter, the passbands and notch stopbands can be tuned over an octave frequency range with minimal impact on performance. Figure 13(a) shows that the notch can be tuned from the frequency where the interfilter transmission line is 99° long to the frequency where it is 261° long while

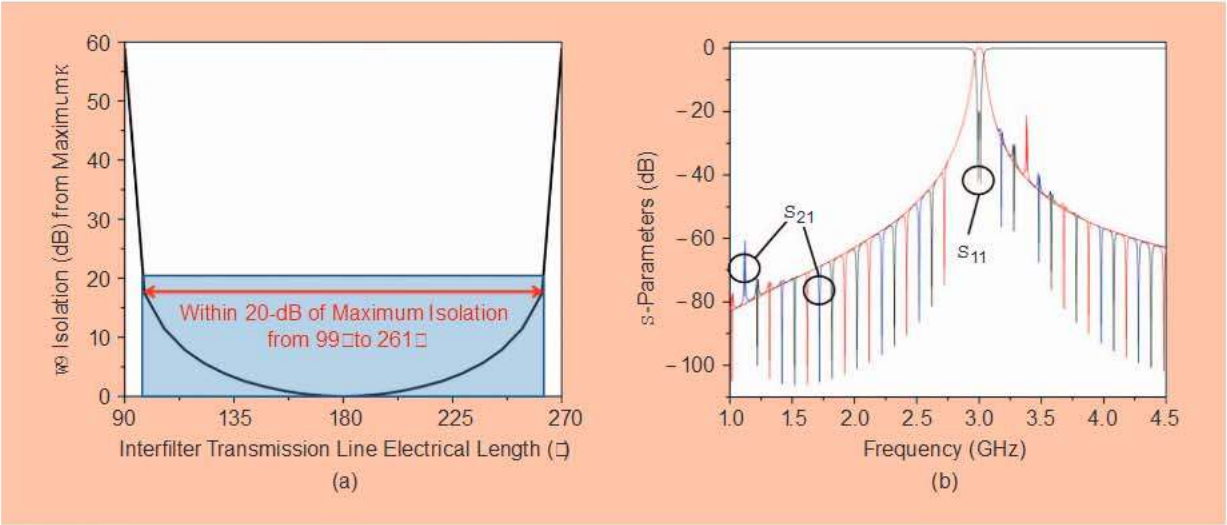

Figure 13. *(a) Change in notch isolation relative to maximum case at the frequency where the interfilter transmission line is 180°. (b) Synthesized superimposed responses showing deep notch isolation at most frequencies and small resonances at frequencies where the transmission line is 90 or 270° long.*

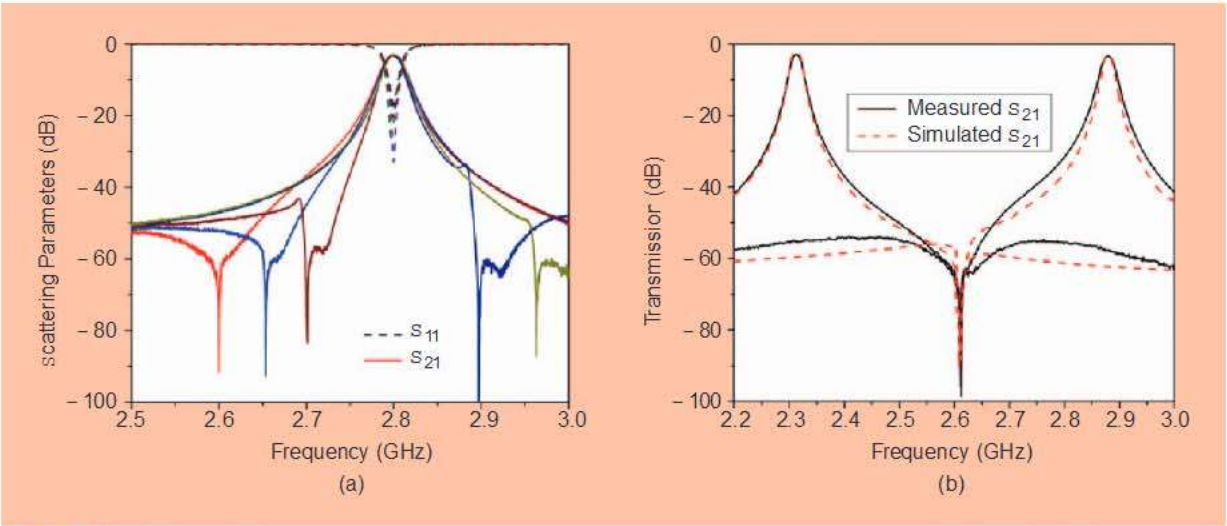

Figure 14. *(a) Measured superimposed responses showing a notch tuning about a static passband. (b) Measured versus simulated transmission response of a bandpass-bandstop filter cascade [14].*

maintaining isolation within 20-dB of the maximum value when it is 180° long.

Figure 13(b) shows the synthesized superimposed responses that were used to extract the data in Figure 13(a). Note that deep additional isolation is present at most notch frequencies, with resonances occurring in designable, narrow frequency bands. Notches with different input impedance in the stopband could be cascaded to enable notches at all frequencies in a bandpass filter's stopband.

Figure 14 shows measured results of the filter cascade described in [14] that verify the targeted deep isolation advantage of bandpass-bandstop filter cascades. Up to 100-dB isolation is achieved over a narrow bandwidth, which has potential to be useful in high dynamic range spectrums and simultaneous transmit and receive systems.

Bandpass-to-Bandstop Filters

The previous section showed that combinations of filters can provide unique responses that are advantageous in some spectral environments. With the high performance of modern switching and tuning elements at RF and microwave frequencies, it has become possible to create filters that can be electronically reconfigured to provide multiple types of frequency responses on demand using a single set of resonators and coupling structures. One example is a filter that can reconfigure its response from a bandpass response to a bandstop one. This reconfiguration capability is shown in Figure 15.

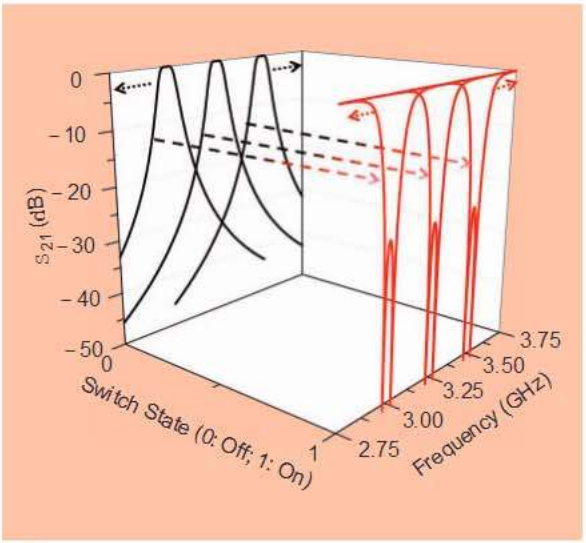

Figure 15. *Conceptual responses from a bandpass-to-bandstop reconfigurable filter. Reconfiguration depends on the state of an electronic switch [30], [31].*

Figure 15 shows conceptual responses from a filter that can both tune its center frequency and response type. The response type depends on the state of an electronic switch. An example of a fabricated filter with this capability can be seen in Figure 16(a). The filter is composed of a layer of Rogers TMM10i substrate that contains the source-to-load transmission line and a Radant RMSW303 switch that is used to toggle the source-to-load coupling from a value of one to a value of approximately zero. Combined with the bandstop response described in [32] and switchable external coupling, this switch enables a bandpass-to-bandstop response and the coupling-routing diagram in Figure 16(b). Note that the external coupling changes as a result of the designed length between the MEMS switch and the coupling slot. The amount of signal reflected to the coupling slot changes when the switch state changes, and therefore the external coupling changes. Bandpass-state measured responses for the filter in Figure 16(a) can be seen in Figure 16(c).

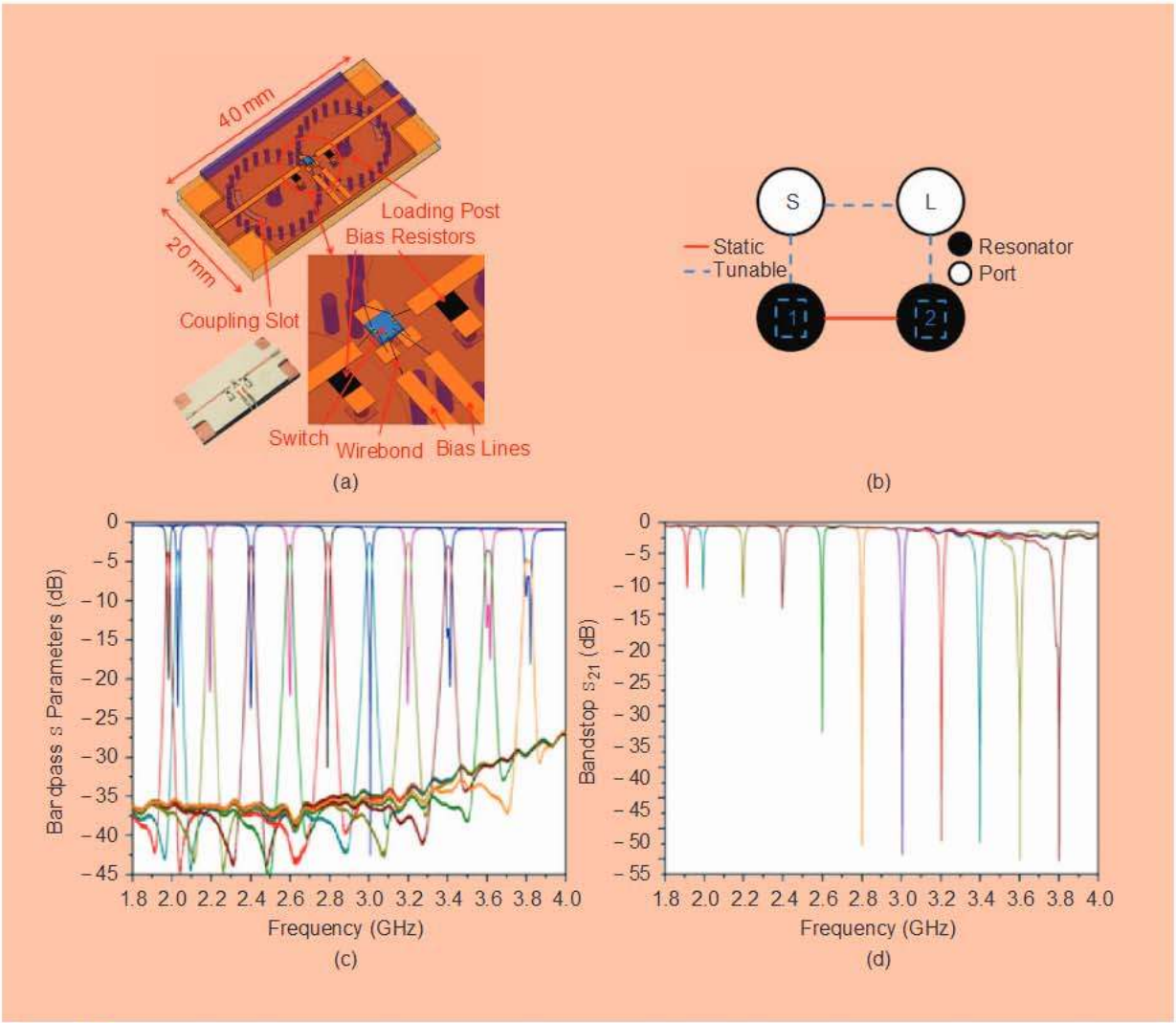

Figure 16. *(a) A model and photograph of fabricated bandpass-to-bandstop filter. (b) A coupling-routing diagram. (c) Measured bandpass responses. (d) Measured bandstop responses.*

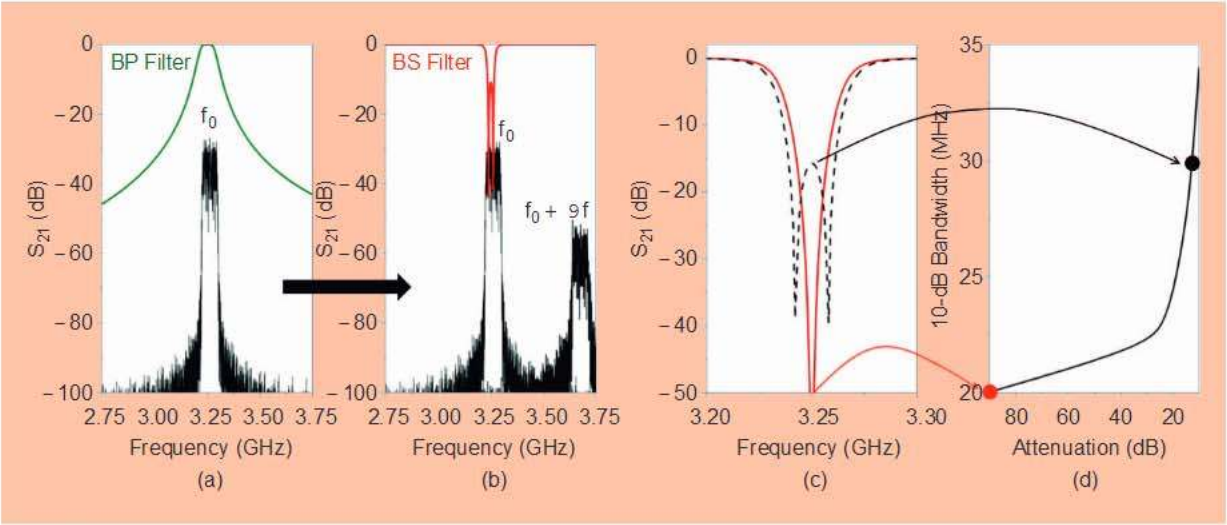

Figure 17. *(a) Bandpass mode receiving signal at f_0. (b) Bandstop mode to quickly receive signal at $f_0 + \Delta f$ (c) and (d) Adjustable bandwidth.*

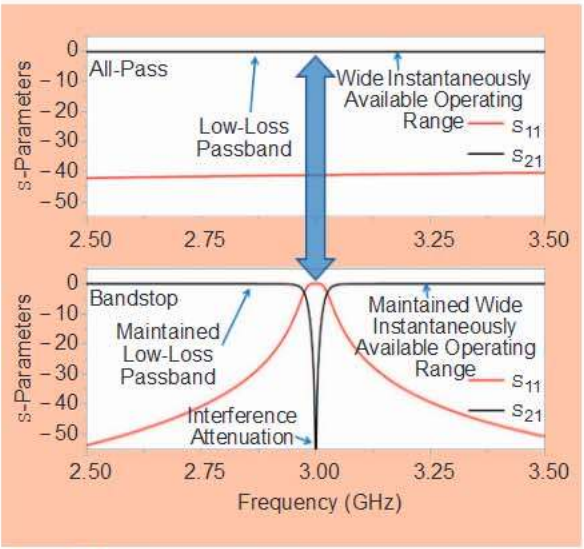

Figure 18. *All-pass and bandstop responses obtained from a switchless filter.*

The filter is capable of tuning from below 2-GHz to 3.8-GHz with a 1.06% fractional bandwidth and 2.4–4.9-dB insertion loss. Stopband isolation is as high as 37-dB. Figure 16(d) shows measured bandstop-state responses for the filter in Figure 16(a), where up to 55-dB attenuation was obtained. Stopband performance of the bandpass filter and passband performance of the bandstop filter near 4-GHz degrade due to poor grounding of the MEMS switch.

Bandpass-to-bandstop filters offer microwave systems interesting, new reconfiguration tradeoffs. For example, if the filter is in bandpass mode receiving a signal at f_0 as in Figure 17(a), and a high-priority signal appears at $f_0 + \Delta f$, it may not be desirable to wait until the bandpass filter can tune to $f_0 + \Delta f$ because important information would be lost. Instead, the filter can quickly switch to bandstop mode to receive the signal at $f_0 + \Delta f$ at the cost of the receiver being open to a wide range of spectrum as shown in Figure 17(b). Another case would be a signal with changing bandwidth. Due to the tunable resonators and coupling theory employed, the bandstop response can reconfigure its bandwidth as shown in Figure 17(c) and (d).

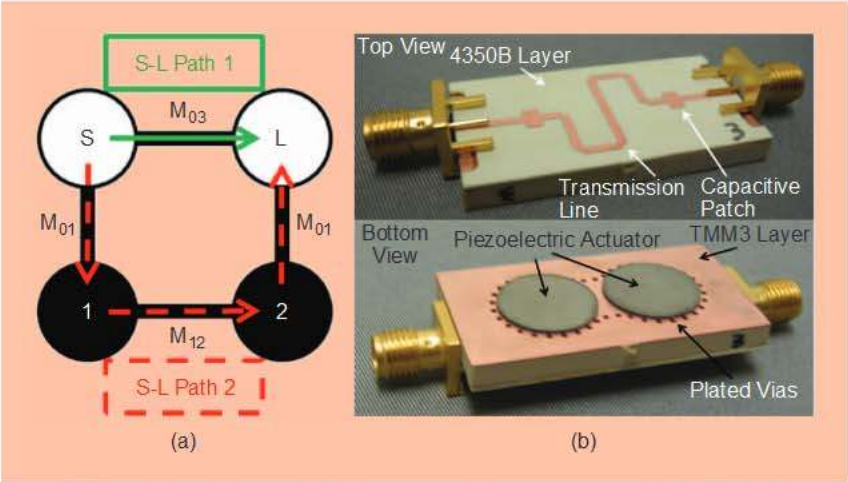

Figure 19. *(a) A coupling-routing diagram and (b) photographs of switchless, tunable bandstop-to-all-pass filter.*

Switchless Bandstop-to-All-Pass Filters

The bandpass-to-bandstop filter could be employed in a system with both narrowband and wideband modes of operation. Some systems that continuously operate over a wide bandwidth would benefit from bandstop filter responses that could be added to a low-loss

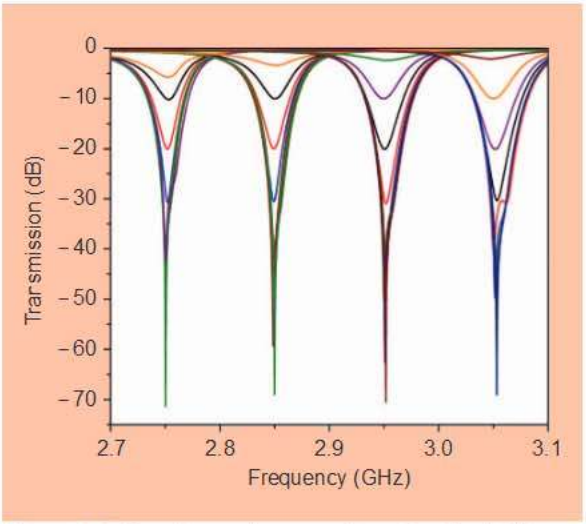

Figure 20. *Superimposed measured results of switchless, tunable bandstop-to-all-pass filter in Figure 19.*

passband on demand and removed when interference subsided. Such systems could use switched bandstop filters to gain this capability, but the switch loss would directly affect the system's passband over the entire bandwidth, reducing system sensitivity. Instead, it would be more beneficial if the filter could reconfigure between bandstop and all-pass responses without the use of switches as shown in Figure 18.

Such a filter can be found in [15], and its coupling-routing diagram and photographs can be seen in Figure 19. The coupling-routing diagram shows that there are two paths from the source port to the load port, and the two paths are the key enabler of a switchless bandstop-to-all-pass response. In the all-pass state, the filter is designed so that the two paths from source to load have the same phase shift when the resonators are tuned to the same frequency. This condition results in constructive interference between the two source-to-load paths, and an ideal all-pass response results if the loss of both paths is the same. To reconfigure the filter to the bandstop response, the resonators must be slightly tuned away from each other in frequency. When the resonators are offset-tuned away from the desired center frequency of a notch response, their off-resonance reactance contributes to the response at the center frequency. Since the resonators are slightly tuned in opposite directions away from the center frequency, a 180° phase difference develops relative to the synchronously tuned case of the all-pass mode. Therefore, the first source-to-load path will become 180° out of phase with the second source-to-load path, and destructive interference will result. If the magnitude of the signals in each path is equal, zero signal will propagate through the filter at the center frequency. Figure 19 shows a substrate-integrated evanescent-mode cavity filter that is tuned using piezoelectric actuators. A transmission line provides one source-to-load path,

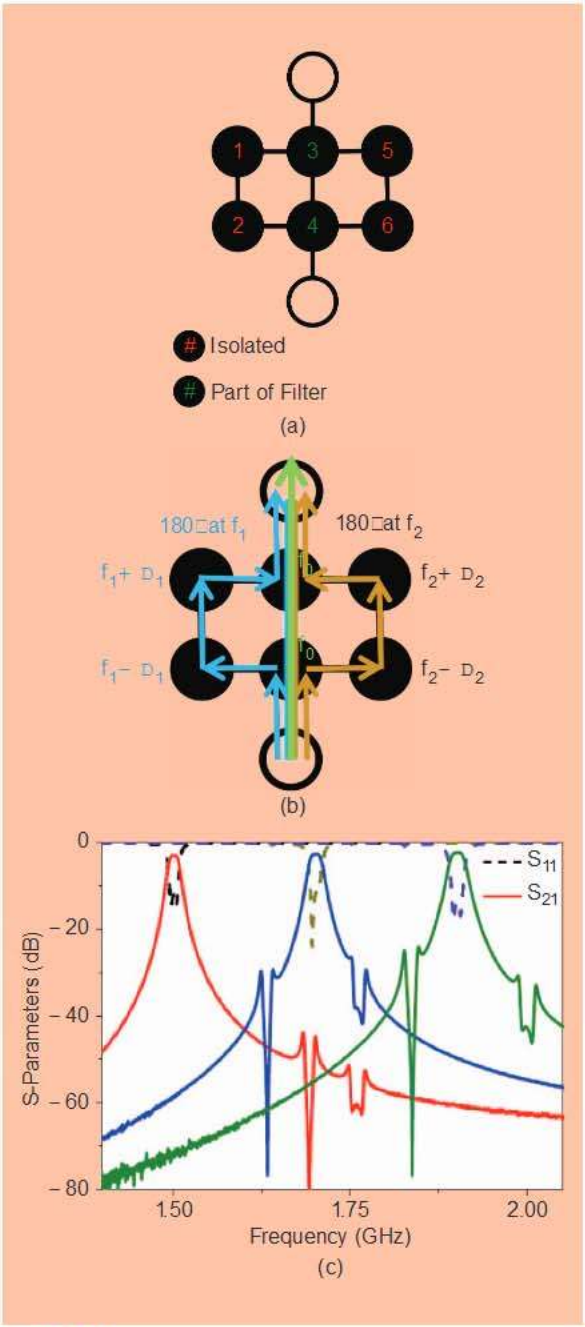

Figure 21. *(a) A six-resonator array configured to produce a two-pole bandpass response. (b) A six-resonator array configured to produce a two-pole bandpass response with two notches in the stopband. (c) Measured response of two-pole passband with two notches in the stopband.*

while coupling through the substrate-integrated resonators provides the other path.

Superimposed measurements of the filter shown in Figure 19 can be seen in Figure 20. The filter is continuously tunable from 2.75-GHz to 3.05-GHz, and continuous variation of the attenuation level from 2.1-dB to over 70-dB is possible at all frequencies in the tuning range. While the resonators have relatively high-Q (540), the resonator source-to-load path has

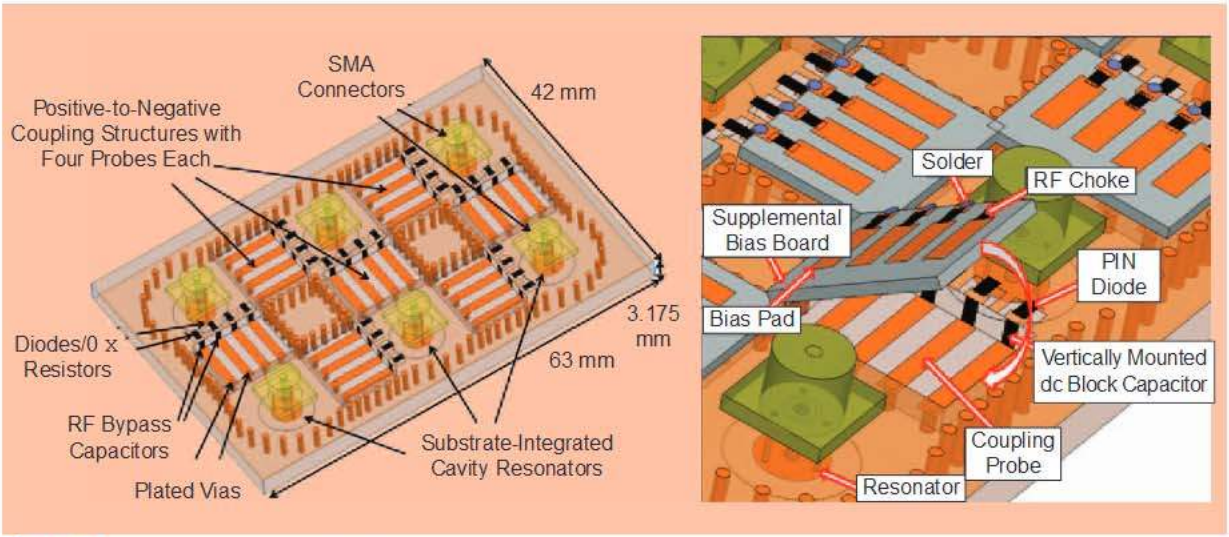

Figure 22. *Simulation model of a six-resonator array of tunable substrate-integrated cavity resonators and positive-to-negative coupling structures.*

more loss than the transmission line source-to-load path, which results in imperfect constructive interference in the all-pass state and a minimum insertion loss of 2.1-dB at the center frequency. Finally, it is important to note that changing between all-pass and bandstop filter shapes requires only very slight frequency tuning of the resonators. Subject to the tuning speed of the resonators used in a particular implementation of a bandstop-to-all-pass filter, the filter shape could be re-optimized very quickly should the spectrum or signals of interest change. Such capability would be useful in wide bandwidth systems that require signal equalization.

Field-Programmable Filter Arrays

Beyond filters that can reconfigure their responses between a few response types, it would be ideal to have a filter that could be reconfigured between any physically possible filter responses on demand. This type of filter is called the field-programmable filter array (FPFA). An FPFA would require complete control of all coupling values between all resonators in the filter. A coupling structure that enables electric field coupling, magnetic field coupling, or a zero coupling state would accomplish this goal. With complete control of coupling values, resonators could be added to or isolated from the circuit on demand, and resonators that are part of the circuit could be used to create any filter response of that order. In addition, resonators could be added into the response in nonstandard ways to produce specialized frequency responses. For example, consider the six-resonator array shown in Figure 21(a) [33].

Figure 21(a) shows a six-resonator FPFA configured to give a two-pole response by isolating four resonators. Figure 21(b) shows that instead of merely isolating resonators 1, 2, 5, and 6, they can be added to the circuit with coupling and tuning specifications that produce notches in the response. A measurement with a two-pole passband that shows this type of response can be seen in Figure 21(c).

A simulation model of the six-resonator array of tunable substrate-integrated evanescent-mode cavity resonators can be seen in Figure 22. Each resonator has a port and is coupled to each adjacent resonator through a switched coupling structure that has ten unique coupling states that include capacitive, inductive, and zero values [33]. A close-up view of a coupling structure can be seen in the right image of Figure 22. The structure implements current probes that reverse the direction of the current in the iris between resonators when they are switched into the circuit, producing a wide array of coupling values [33].

The FPFA in Figure 22 is capable of multiple other response types. Figure 23(a) shows four-pole responses that were obtained by isolating resonators 5 and 6 with zero coupling. The FPFA is capable of adding and removing transmission zeros to this response on demand, enabling a dynamic isolation-group delay tradeoff that can be optimized for the current situation.

The FPFA shown in Figure 22 can be accurately modeled with the coupling matrix. Figure 23(b) shows measured versus synthesized responses of the FPFA, where the synthesized response uses the bandwidth and frequency scaled version of the $\mathbf{M}$ matrix in (5). Note that the $\mathbf{M}$ values in (5) are set to values that were extracted from measurement of a weakly coupled set of two resonators. A combination of measurement and synthesis enables one to determine all of the available responses that an FPFA can provide for the optimization of a system's front-end frequency response.

$$
\begin{bmatrix}
0 & 0 & 0 & 0.841 & 0 & 0 & 0 & 0 \\
0 & 6.820 & 0.649 & 0.649 & 0 & 0 & 0 & 0 \\
0 & 0.649 & 6.820 & 0 & 0.649 & 0 & 0 & 0 \\
0.841 & 0.649 & 0 & 0 & 0.649 & 0.649 & 0 & 0 \\
0 & 0 & 0.649 & 0.649 & 0 & 0 & 0.649 & 0.841 \\
0 & 0 & 0 & 0.649 & 0 & -5.270 & 0.649 & 0 \\
0 & 0 & 0 & 0 & 0.649 & 0.649 & -6.370 & 0 \\
0 & 0 & 0 & 0 & 0.841 & 0 & 0 & 0
\end{bmatrix} \quad (5)
$$

We are in the post tunable-filter era. Transfer-function-adaptive filters can now be designed and implemented.

of this technique will depend on the overall robustness and stability of the filter. On the other hand, closed-loop control may be preferable when the highest possible performance is required. Nevertheless, this may come with increased power requirements and system complexity. Reliability and stability of the RF MEMS tuners

Conclusion and Future Steps

The evanescent-mode tunable filter RF MEMS technology has matured and scales favorably at least up to W band. This technology has showed consistent high-Q performance (>400–1,000) and wide tuning range (>2:1) from L- to W-band. Besides frequency-agile filters, a number of new filter synthesis techniques have been developed that allow in-the-field reconfiguration of the filter transfer function. This includes center frequency control, bandwidth control, and dynamic allocation of transmission zeros at arbitrary frequencies. Furthermore, bandpass-to-bandstop transformations with tunable resonator arrays and switchable coupling sections have been demonstrated. Such concepts have also been extended to field-programmable filter-arrays with reconfigurable coupling structures that enable electric field coupling, magnetic field coupling, or zero coupling states.

These important advances have opened the door for some areas of research to become particularly relevant today. The first one is related to controlling these filters. Open- or closed-loop control could be preferable depending on the performance requirements and power budget of the system. Open-loop control could be based on simple look-up tables that may need to be compensated for temperature variations. However, the effectiveness

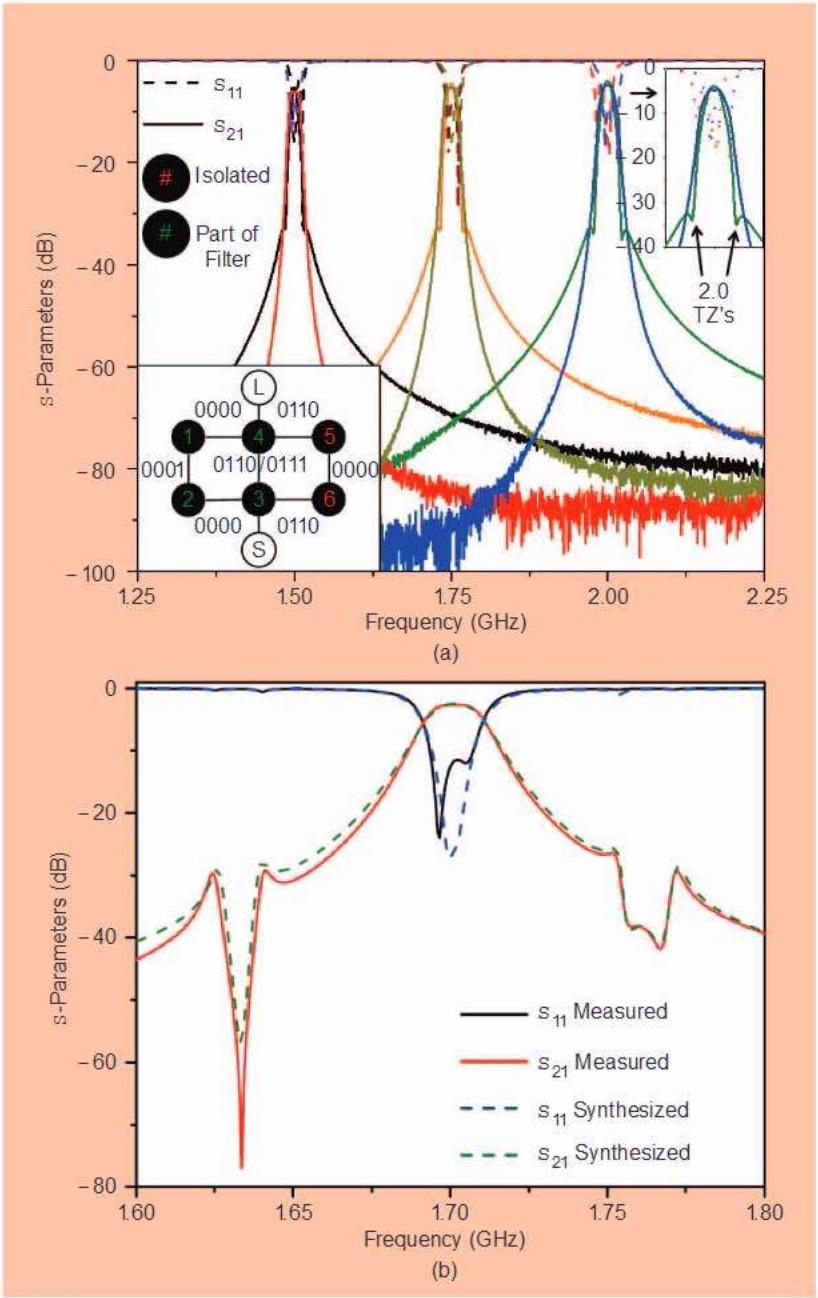

Figure 23. *(a) Four-pole responses obtained from the circuit in Figure 22 by isolating resonators 5 and 6. Responses with and without transmission zeros are obtained by toggling the coupling between resonators 3 and 4 between capacitive and inductive values. (b) Measured versus synthesized responses.*

Tunable evanescent-mode filters are capable of providing wide tunability, high selectivity, and low loss while maintaining narrow bandwidths.

is a key determining factor in the issue of control for such filters. Preliminary results are very encouraging in this area. Specifically, it seems that after an initial burn-in period, even gold-based tuners tend to remain stable for over 100 million cycles [27]. Lack of contact-induced failures and the anticipated rapid growth in this area are expected to improve these significantly.

Power handling, linearity, vibration, and tuning speed are also areas of significant interest in these filters. All these requirements are tightly interlinked and often need to be simultaneously considered. For example, linearity depends on the applied RF power to the filter and the desired tuning range. Tuning speed is a function of the filter's unloaded quality factor and desired tuning range. In addition to the above, the following general comments can also be made:

- *Power handling*: The maximum RF power is primarily limited by two phenomena: nonlinear electromechanical coupling [23], [34]–[36] and RF gas discharge [37]–[39]. Nonlinear electromechanical coupling is a direct consequence of the fact that the RF MEMS tuners in evanescent-mode resonators are subject to both bias-induced (electrostatic or piezoelectric) and RF voltage-induced forces. For low power levels this coupling is not significant. However, when the RF power approaches the 0.5–10 W level (for filters with over 2:1 tuning range and reasonable bias voltages in the 100–200 V range), this coupling becomes significant and results in a bifurcated frequency response. RF gas discharge is not as well understood and more research is required to establish solid design criteria. Existing results suggest that these filters can handle several W of RF power before RF gas discharge becomes important [35].
- *Linearity*: Evanescent-mode filters are, in general, very linear filters with IIP3 levels in excess of 50 dBm [34]. Similarly to power handling, however, linearity depends on the filter topology as well. Most of the filters that have been designed today have not optimized their topology to achieve the maximum possible power handling and linearity by equalizing the RF voltages of their individual resonators. Consequently, it is expected that few resonators of a particular filter topology will determine the power handling and linearity of the filter. Future research efforts can investigate functionality and adaptivity versus linearity and power handling tradeoffs.
- *Vibration*: Vibration and shock considerations become important in evanescent-mode filters due to the potential microphonics effects. Recent research [40]–[42] has shown that vibration levels of 1–2 g could result in sideband levels of 40–50 dBc depending on the design. However, significant improvement by at least 25-dB can be achieved by properly modifying the applied bias signal to counteract the vibration effects [42]. Additional research is needed to optimize these counteracting mechanisms and potentially include them in closed-feedback loops particularly in systems suffering from strong vibration effects.
- *Tuning speed*: Tuning speed is primarily limited by the mass of a tuner, its aerodynamic damping, and the applied bias waveform. Relatively large membranes with diameters of over 1 mm typically result in tuning speeds of over 100–200 ns. This speed can be substantially reduced to less than 10 ns (actuation time) and 60 ns (release time) if the membrane is replaced by an array of small beams and the appropriate bias waveform is applied [43]. Although this does not substantially impact the resonator's quality factor, it typically results in reduced tuning range due to the smaller beam deflections. Further research is required to achieve lower speeds and/or improve the tuning range for fast tuners. While it may not be possible to approach the speed of solid-state varactor-tuned filters [46], it will likely become comparable to the one provided by fast RF MEMS switches for the same tuning range [47] with the additional advantage of significantly higher Q.

While the above comments show the interdependence of the major filter characteristics, they also underline the fact that there is room for design tradeoffs to simultaneously achieve the desired filter characteristics.

References

[1] G. F. Craven and C. K. Mok, "The design of evanescent mode waveguide bandpass filters for a prescribed insertion loss characteristic," *IEEE Trans. Microwave Theory Tech.*, vol. 19, no. 3, pp. 295–308, Mar. 1971.

[2] M. S. Arif and D. Peroulis, "A 6 to 24-GHz continuously tunable, microfabricated, high-Q cavity resonator with electrostatic MEMS actuation," in *IEEE MTT-S Int. Microwave Symp. Dig.*, June 2012, pp. 1–3.

[3] E. J. Naglich, J. Lee, and D. Peroulis, "Tunable bandstop filter with a 17-to-1 upper passband," in *IEEE MTT-S Int. Microwave Symp. Dig.*, June 2012, pp. 1–3.

[4] X. Liu, L. P. B. Katehi, W. J. Chappell, and D. Peroulis, "High-Q tunable microwave cavity resonators and filters using SOI-based RF MEMS tuners," *IEEE/ASME J. Microelectromech. Syst.*, vol. 19, no. 4, pp. 774–784, Aug. 2010.

[5] S. Moon, H. H. Sigmarsson, H. Joshi, and W. J. Chappell, "Substrate integrated evanescent-mode cavity filter with a 3.5 to 1 tuning ratio," *IEEE Microwave Wireless Compon. Lett.*, vol. 20, no. 8, pp. 450–452, Aug. 2010.

[6] H. Joshi, H. H. Sigmarsson, S. Moon, D. Peroulis, and W. J. Chappell, "Tunable high Q narrow-band triplexer," in *IEEE MTT-S Int. Microwave Symp. Dig.*, June 2009, pp. 1477–1480.

[7] G. Craven and C. Radcliffe, "Microwave filters for communication satellites," *IEE J. Microwaves, Opt. Acoust.*, vol. 2, no. 5, pp. 167–175, Sept. 1978.

[8] C. K. Mok, "Design of evanescent-mode waveguide diplexers," *IEEE Trans. Microwave Theory Tech.*, vol. 21, no. 1, pp. 43–48, Jan. 1973.

[9] X. Gong, A. Margomenos, B. Liu, W. J. Chappell, and L. P. B. Katehi, "High-Q evanescent-mode filters using silicon micromachining and polymer stereolithography processing," in *IEEE MTT-S Int. Microwave Symp. Dig.*, June 2004, pp. 433–436.

[10] H. Joshi, H. H. Sigmarsson, D. Peroulis, and W. J. Chappell, "Highly loaded evanescent cavities for widely tunable high-Q filters," in *IEEE MTT-S Int. Microwave Symp. Dig.*, June 2007, pp. 2133–2136.

[11] H. Joshi, H. H. Sigmarsson, S. Moon, D. Peroulis, and W. J. Chappell, "High Q fully reconfigurable tunable bandpass filters," *IEEE Trans. Microwave Theory Tech.*, vol. 57, no. 12, pp. 3525–3533, Dec. 2009.

[12] X. Liu, L. P. B. Katehi, W. J. Chappell, and D. Peroulis, "A 3.4–6.2-GHz continuously tunable electrostatic MEMS resonator with quality factor of 460–530," in *IEEE MTT-S Int. Microwave Symp. Dig.*, Boston, MA, June 2009, pp. 1149–1152.

[13] E. J. Naglich, J. Lee, D. Peroulis, and W. J. Chappell, "Tunable, substrate integrated, high Q filter cascade for high isolation," in *IEEE MTT-S Int. Microwave Symp. Dig.*, June 2010, pp. 1468–1471.

[14] E. J. Naglich, J. Lee, D. Peroulis, and W. J. Chappell, "Bandpass-bandstop filter cascade performance over wide frequency tuning ranges," *IEEE Trans. Microw. Theory Tech.*, vol. 58, no. 12, pp. 3945–3953, Dec. 2010.

[15] E. J. Naglich, J. Lee, D. Peroulis, and W. J. Chappell, "Switchless tunable bandstop-to-all-pass reconfigurable filter," *IEEE Trans. Microw. Theory Tech.*, vol. 60, no. 5, pp. 1258–1265, May 2012.

[16] E. J. Naglich, J. Lee, D. Peroulis, and W. J. Chappell, "High-Q tunable bandstop filters with adaptable bandwidth and pole allocation," in *IEEE MTT-S Int. Microwave Symp. Dig.*, June 2011, pp. 1–4.

[17] K. Chen, J. Lee, W. J. Chappell, and D. Peroulis, "Co-design of highly efficient power amplifier and high-Q output bandpass filter," *IEEE Trans. Microw. Theory Tech.*, vol. 61, no. 11, pp. 3940–3950, Nov. 2013.

[18] R. Stefanini, J. D. Martinez, M. Chatras, A. Pothier, V. E. Boria, and P. Blondy, "Ku band high-Q tunable surface-mounted cavity resonator using RF MEMS varactors," *IEEE Microwave Wireless Compon. Lett.*, vol. 21, no. 5, pp. 237–239, May 2011.

[19] S.-J. Park, I. Reines, C. Patel, and G. M. Rebeiz, "High-Q RF-MEMS 4–6-GHz tunable evanescent-mode cavity filter," *IEEE Trans. Microwave Theory Tech.*, vol. 58, no. 2, pp. 381–389, Feb. 2010.

[20] V. Sekar, M. Armendariz, and K. Entesari, "A 1.2–1.6-GHz substrate-integrated-waveguide RF MEMS tunable filter," *IEEE Trans. Microwave Theory Tech.*, vol. 59, no. 4, pp. 866–876, Apr. 2011.

[21] W. D. Yan and R. R. Mansour, "Tunable dielectric resonator bandpass filter with embedded MEMS tuning elements," *IEEE Trans. Microwave Theory Tech.*, vol. 55, no. 1, pp. 154–160, Jan. 2007.

[22] F. Huang, S. Fouladi, and R. R. Mansour, "High-Q tunable dielectric resonator filters using MEMS technology," *IEEE Trans. Microwave Theory Tech.*, vol. 59, no. 12, pp. 3401–3409, Dec. 2011.

[23] P. Blondy and D. Peroulis, "Handling RF power," *IEEE Microwave Mag.*, vol. 14, no. 1, pp. 24–38, Jan. 2013.

[24] M. S. Arif and D. Peroulis, "All-silicon technology for high-Q evanescent mode cavity tunable resonators and filters," *IEEE/ASME J. Microelectromech. Syst.*, vol. PP, no. 99, pp. 1–13.

[25] E. Naglich, S. Moon, and M. Sinani, "High-Q MEMS-tunable W-band bandstop resonators," in *IEEE MTT-S Int. Microwave Symp. Dig.*, June 2014, pp. 1–4.

[26] A. Atia, A. Williams, and R. Newcomb, "Narrow-band multiple-coupled cavity synthesis," *IEEE Trans. Circuits Syst.*, vol. 21, pp. 649–655, Sept. 1974.

[27] Z. Yang and D. Peroulis, "A 23-35-GHz MEMS tunable all-silicon cavity filter with stability characterization up to 140 million cycles," in *IEEE MTT-S Int. Microwave Symp. Dig.*, June 2014, pp. 1–4.

[28] M. S. Arif and D. Peroulis, "All-Silicon tunable cavity filters for microwave and millimeter-wave applications," *IEEE Trans. Microw. Theory Tech.*, May 2013, to be published.

[29] H. Joshi, "Multi band RF bandpass filter design," Ph.D. dissertation, School of Elect. and Comput. Eng., Purdue Univ., West Lafayette, IN, 2010.

[30] E. Naglich, J. Lee, D. Peroulis, and W. Chappell, "A tunable bandpass-to-bandstop reconfigurable filter with independent bandwidths and tunable response shape," *IEEE Trans. Microwave Theory Tech.*, vol. 58, pp. 3770–3779, Dec. 2010.

[31] E. J. Naglich and W. J. Chappell, "Dynamic spectrum utilization and performance enhancement of tunable bandpass-to-bandstop reconfigurable filters using advanced MEMS switches," in *Proc. Government Microcircuit Applications Critical Technology Conf.*, Orlando, FL, Mar. 2011.

[32] J. Lee, E. Naglich, and W. Chappell, "Frequency response control in frequency-tunable bandstop filters," *IEEE Microwave Wireless Compon. Lett.*, vol. 20, pp. 669–671, Dec. 2010.

[33] E. J. Naglich, D. Peroulis, and W. J. Chappell, "Low-order filter response enhancement in reconfigurable resonator arrays," *IEEE Trans. Microwave Theory Tech.*, vol. 61, pt. 2, no. 12, pp. 4387–4395, Dec. 2013.

[34] X. Liu, L. P. B. Katehi, W. J. Chappell, and D. Peroulis, "Power handling of electrostatic MEMS evanescent-mode (EVA) tunable bandpass filters," *IEEE Trans. Microwave Theory Tech.*, vol. 60, no. 2, pp. 270–283, Feb. 2012.

[35] K. Chen, H. Sigmarsson, and D. Peroulis, "Power handling of high-Q evanescent-mode tunable filter with integrated piezoelectric actuators," in *IEEE MTT-S Int. Microwave Symp. Dig.*, Montreal, QC, Canada, June 2012, pp. 1–3.

[36] X. Liu, E. J. Naglich, and D. Peroulis, "Non-linear effects in MEMS tunable bandstop filters," in *IEEE MTT-S Int. Microwave Symp. Dig.*, Montreal, QC, Canada, June 2012, pp. 1–8.

[37] A. Semnani, V. Ayyaswamy, A. A. Alexeenko, and D. Peroulis, "Pre-breakdown evaluation of gas discharge mechanisms in microgaps," *Appl. Phys. Lett.*, vol. 102, no. 17, pp. 17410–174102-4, Apr. 2013.

[38] A. Semnani, K. Chen, and D. Peroulis, "Microwave gas breakdown in tunable evanescent-mode cavity resonators," *IEEE Microwave Wireless Compon. Lett.*, vol. 24, no. 5, pp. 351–353, Feb. 2014.

[39] A. Semnani, V. Ayyaswamy, A. A. Alexeenko, and D. Peroulis, "Frequency response of atmospheric pressure gas breakdown in micro/nanogaps," *Appl. Phys. Lett.*, vol. 103, no. 6, pp. 063102–063102-4, Aug. 2013.

[40] X. Liu, J. Small, D. Berdy, L. P. B. Katehi, W. J. Chappell, and D. Peroulis, "Impact of mechanical vibration on the performance of RF MEMS evanescent-mode tunable resonators," *IEEE Microwave Wireless Compon. Lett.*, vol. 21, no. 8, pp. 406–408, Aug. 2011.

[41] K. Chen, X. Liu, A. Kovacs, W. J. Chappell, and D. Peroulis, "Anti-biased electrostatic RF MEMS varactors and tunable filters," *IEEE Trans. Microwave Theory Tech.*, vol. 58, no. 12, pt. 2, pp. 3971–3981, Dec. 2010.

[42] M. A. Khater and D. Peroulis, "Vibration mitigation for evanescent-mode cavity filters," in *IEEE MTT-S Int. Microwave Symp. Dig.*, Tampa, FL, June 2014, pp. 1–3.

[43] J. Small, M. S. Arif, A. Fruehling, and D. Peroulis, "A tunable miniaturized RF MEMS resonator with simultaneous high Q (500–735) and fast response speed (< 10-60 μs)," *IEEE/ASME J. Microelectromech. Syst.*, vol. 22, no. 2, pp. 395–405, Apr. 2013.

[44] F. Huang, W. D. Yan, and R. R. Mansour, "High-Q narrowband tunable combline bandpass filters using MEMS capacitor banks and piezomotors," *IEEE Trans. Microwave Theory Tech.*, vol. 61, no. 1, pp. 393–402, Jan. 2013.

[45] W. D. Yan and R. R. Mansour, "Micromachined millimeter-wave ridge waveguide filter with embedded MEMS tuning elements," in *IEEE MTT-S Int. Microwave Symp. Dig.*, June 2006, pp. 1290–1293.

[46] A. R. Brown and G. M. Rebeiz, "A varactor-tuned RF filter," *IEEE Trans. Microwave Theory Tech.*, vol. 48, no. 7, pp. 1157–1160, July 2000.

[47] M. A. El-Tanani and G. M. Rebeiz, "High-performance 1.5–2.5-GHz RF-MEMS tunable filters for wireless applications," *IEEE Trans. Microwave Theory Tech.*, vol. 58, no. 6, pp. 1629–1637, June 2010.